IEEE Access
Multidisciplinary | Rapid Review | Open Access Journal

SPECIAL SECTION ON ANTENNA AND PROPAGATION FOR 5G AND BEYOND

Received November 6, 2019, accepted December 1, 2019, date of publication December 10, 2019,
date of current version December 26, 2019.

Digital Object Identifier 10.1109/ACCESS.2019.2958897

MIMO Antenna System for Multi-Band Millimeter-Wave 5G and Wideband 4G Mobile Communications

EMAD AL ABBAS[1,2], (Student Member, IEEE),
MUHAMMAD IKRAM[1], (Student Member, IEEE),
AHMED TOAHA MOBASHSHER[1], (Member, IEEE),
AND AMIN ABBOSH[1], (Senior Member, IEEE)

[1]School of Information Technology and Electrical Engineering (ITEE), The University of Queensland, Brisbane, QLD 4072, Australia
[2]Electrical Engineering Department, University of Baghdad, Baghdad 10071, Iraq

Corresponding author: Emad Al Abbas (e.alabbas@uq.ed.au)

This work was supported by the Australian Research Council under Grant ARC LP160100917.

ABSTRACT A multiple-input multiple-output (MIMO) antenna system is proposed for fifth generation (5G) and fourth generation (4G) mobile communication. The design meets all of the requirements of both 5G and 4G antennas using only a single structure. Since 5G will work at millimeter-wave (mm-Wave), the proposed design serves triple bands at mm-Wave (28, 37 and 39 GHz) for 5G in addition to 2 GHz band (1.8-2.6) for 4G. Each MIMO element consists of a slot-based antenna, fed by two microstrip feeders for the 5G and 4G bands. The design works as a tapered slot antenna at mm-Wave offering end-fire radiation for 5G and works as an open-ended slot antenna for a 2 GHz band offering omni-direction radiation for 4G. The slot antenna type used in the proposed design produces wide bandwidths for the 5G and 4G. The overall volume of each MIMO antenna element is $0.21 \times 0.10 \times 0.003\ \lambda^3$, where λ is the wavelength of the lowest operating frequency. As a proof of concept, a prototype is developed and tested. The measured results show a wide impedance bandwidth of $|S_{11}|<$ -10 dB covering the band 27.5-40 GHz for 5G, and impedance bandwidth of $|S_{11}| <$ -6 dB covering the band 1.8-2.6 GHz for 4G.

INDEX TERMS 5G, 4G, MIMO antenna, mobile communication, slot antenna.

I. INTRODUCTION

Multiple -input multiple-output (MIMO) antenna systems are seen as a key technology for an upcoming fifth generation (5G) and the existing fourth generation (4G) mobile antenna system to enhance the data rate [1]–[4]. Along with MIMO antenna system, 5G requires a wide bandwidth to maximize the data rate. Unfortunately, the current available bandwidth at sub-3 GHz is congested [5], thus, many international organizations assigned the millimeter wave band (mm-Wave), which includes 28, 37 and 39 GHz as a potential frequency band for 5G [6], [7]. Therefore, the current mobile terminals need to support 5G at mm-Wave band in addition to the existing 4G at sub-3 GHz band. However, mobile terminals have limited space and adding many antennas is not preferred. Thus, the solution is to develop a MIMO antenna system having antenna elements covering different bands of 5G and 4G by using a single structure rather than two. In other words, the usage of multi-band antenna elements in the MIMO system is a key factor to reduce the antenna footprint inside the mobile terminal [5], [6], [8], [9]. However, integration of 5G and 4G antennas in the same structure produces many challenges in terms of antenna size, isolation between antennas at different bands, and antenna gain.

Recently, some research efforts have been invested to satisfy the 4G and/or 5G antenna requirements for MIMO application at the sub-6 GHz band. T-shaped or coupled-feed approaches were investigated in [2], [10]–[12] at the sub-6 GHz spectrum for 5G or 4G applications. 5G and 4G antenna models for Long Term Evolution (LTE) bands 42/43 and LTE band 46 were proposed utilizing a bent strip structure in [13] or inverted L-shaped open slot antenna [14]. In addition, a number of promising 5G (above 6-GHz) and 4G (sub-3 GHz) MIMO systems also exist, which utilize separate antenna structures for 5G and 4G [15], [16], or a single large antenna footprint with multiple bands [9]. Unfortunately,

The associate editor coordinating the review of this manuscript and approving it for publication was Qammer Hussain Abbasi.

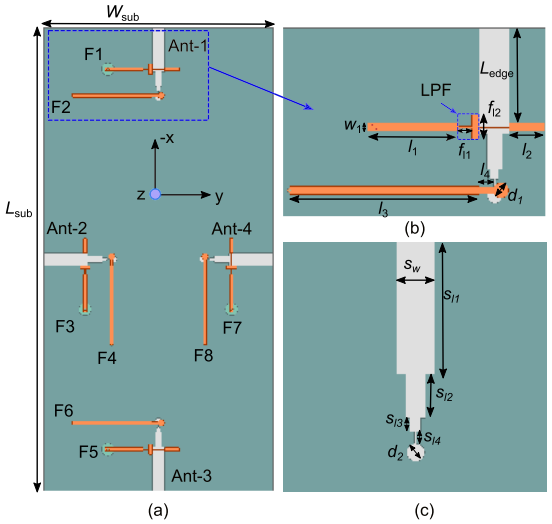

FIGURE 1. The geometry of 4-element MIMO antenna system. (a) Top view (full design), (b) Ant-1 (large view), and (c) tapered slot in the ground plane: Final optimized parameters with their values for MIMO antenna system are: $L_{sub} = 158$, $W_{sub} = 77.8$, $fl_1 = 1.89$, $fl_2 = 3.5$, $l_1 = 13$, $l_2 = 4.95$, $l_3 = 27$, $l_4 = 2$, $d_1 = 2$, $L_{edge} = 13.5$ and $w_1 = 1.17$, all values are in millimeter (mm).

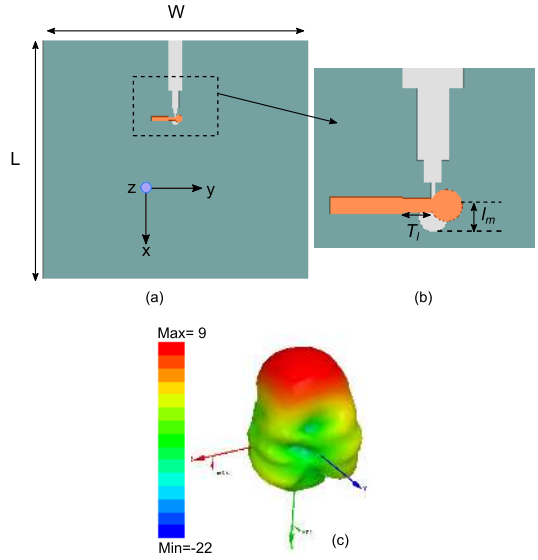

FIGURE 2. The geometry of 5G antenna. (a) Top view, (b) Large view, and (c) 3D realized gain in dBi.

those reported designs either do not support the mm-Wave frequency band 5G [2], [9]–[15] or require extra space from the scarce real estate of the mobile terminal [16].

In this paper, an integrated 4-element 5G/4G MIMO antenna system using a novel, single antenna structure is presented. It works at triple bands (28, 37 and 39 GHz) for 5G and the wideband (1.8-2.6 GHz) for 4G. Each MIMO element consists of a slot in the ground plane and two microstrip feeding ports in the top layer; a low pass filter (LPF) is also integrated into the structure for isolation enhancement. By properly feeding the antennas from one of two ports, the antenna can work in two different operating modes. One of the feeding ports corresponds to a tapered slot antenna with end-fire radiation for 5G, whilst the other feeding port corresponds to an open-ended slot antenna with omni-direction radiation at 4G. MIMO performance factors are also calculated and discussed.

II. PROPOSED MIMO ANTENNA SYSTEM DESIGN

The geometry of the complete MIMO antenna system is shown in Fig.1. It is modelled and simulated using High Frequency Structure Simulator (HFSS). An RT/duroid-5880 substrate ($\epsilon_r = 2.2$, $\tan\delta = 0.0009$ and thickness $t = 0.381$ mm) with the overall size of $L_{sub} \times W_{sub}$ mm^2 is used to print the antenna structure due its low dielectric losses. All antenna elements (Ant-1-Ant-4) are realized on the four sides of the substrate as a proof of concept. All microstrip feeding lines are placed on the top layer, while tapered slots are etched in the ground plane located at the bottom layer of the substrate.

The antenna structure is more suitable for future 5G/4G applications, owing to the dual functionality of the ground slot. First, when the slot is fed from the edge (F2 for example), it works as a tapered slot antenna. In this case, the signal propagates via a symmetrical tapered slot line and gives end-fire radiation patterns with high gain, satisfying the requirements of 5G at mm-Waves [17]. Second, when it is fed from the center (F1 for example), it works as an open-ended slot antenna and gives an omni-directional radiation satisfying the requirements of 4G at 2 GHz band. Accordingly, a single antenna, having a small footprint compared with separate antennas, can be designed to meet the requirements of low and high frequency bands. A detailed discussion on the design procedure and construction approach of the proposed antenna structure is given in the following sections.

A. MULTI-BAND 5G ANTENNA STRUCTURE

The structure of the 5G antenna is shown in Fig. 2. It consists of a tapered slot, which enables wideband performance, and microstrip feed line [17]. The total size of the single element with the ground plane is 70×77.8 mm^2 ($L \times W$). The narrower edge of the tapered slot is ended with a $\lambda_g/4$ circular stub. The diameter of the stub is d_2 (Fig. 1(b)). The tapered slot is fed via a circular sector microstrip line with diameter d_1. The circular sector is connected to a 50 Ω transmission line through an impedance matching transformer that has a total length of T_l. The circular stub of the slot and circular sector of the feed line contribute to provide a broadband impedance matching bandwidth [18]. Final optimized parameters (as shown in Fig. 1(c)) for the tapered slot are as follow: $s_{l1} = 15$, $s_{l2} = 5$, $s_{l3} = 1.5$, $s_{l4} = 1.42$, $d_2 = 2$, $s_w = 4.2$, $T_l = 2$ and $l_m = 1.9$, all values are in mm.

B. INTEGRATION OF 4G FEEDING STRUCTURE TO 5G ANTENNA STRUCTURE

In this part, the same tapered slot which was used for 5G band in the previous section is also used to cover the low frequency band for 4G. This dual feature of the slot fulfils the requirements of dual wireless standards (5G/4G). The feeder

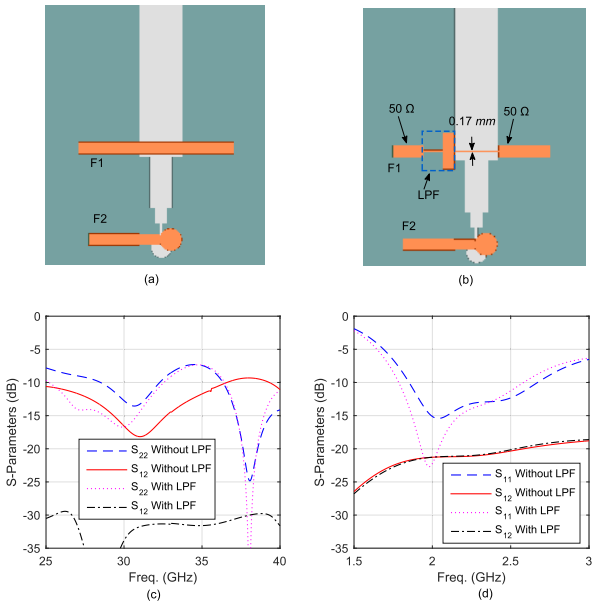

FIGURE 3. (a) Integrated antenna structure without low pass filter, (b) with low pass filter, (c) 5G reflection coefficient without/with low pass filter, and (d) 4G reflection coefficient without/with low pass filter.

(F_1) is used to excite the tapered slot which works as an open-ended slot antenna, as shown in Fig. 3. The 4G feeding structure started first with a simple 50 Ω microstrip transmission line (Fig. 3(a)), while the final optimized feeding structure consists of a low pass filter (LPF) and a modified transmission line, as shown in Fig. 3(b) along with the 5G antenna. Where, F_1 is used to excite the slot as an open-ended slot antenna and F_2 is used to excite the same slot as a tapered slot antenna. It covers a low frequency band from 1.8-2.6 GHz and a high frequency band from 25-40 GHz. The length of the open-ended slot is 24.92 mm ($s_{l1} + s_{l2} + s_{l3} + s_{l4} + d_2$) which is $\lambda_g/4$ at 2 GHz (λ_g is guided wavelength).

The addition of the 4G feeder (F_1) to the tapered slot degrades the performance of the 5G antenna in terms of impedance matching, isolation and gain. To understand the performance degradation of the 5G antenna, a study is conducted in four stages ($Stage_1$-$Stage_4$) based on the current distributions in the following sub-sections.

1) STAGE 1

Before adding the 4G feeder, the current distribution of the 5G antenna is shown in Fig. 4(a). It can be seen that the current is mainly propagating towards the open end of the slot and radiates as a tapered slot antenna. It covers 25-40 GHz band, with a maximum gain of 9.14 dBi at 38 GHz.

2) STAGE 2

After adding the 4G feeder, the coupling is found to be high between the 4G and 5G feeders as shown in Fig. 4(b). The 4G feeder works as a shunt impedance or a signal blocker for the 5G antenna signal propagation. As a result, the main current propagates toward the upper and lower side of 4G micorstrip feeder instead of propagating toward the open-end of the slot. At this stage, s-parameters of the antenna at high and low frequencies are shown in Fig. 3(c) and Fig. 3(d) without the LPF. It covers 28.5-32.5 and 36-40 GHz while the maximum gain is observed to be 5.87 dBi. It can be noticed that after adding the 4G feeder, gain and impedance matching is reduced, and the isolation is also poor.

3) STAGE 3

To minimize the effect of the 4G feeder on the 5G band, the equivalent shunt impedance of the 4G feeder should be increased, so it works as an open circuit for the 5G signal. By doing this, the coupling between F_1 and F_2 can be reduced significantly [19] and the performance of the antenna can be improved. The shunt impedance can be increased by reducing the width of the 4G feeder above the slot, as shown in Fig. 4(c). However, due to fabrication process limitations, the width of the 4G feeder is reduced only to 0.17 mm as shown in Fig. 3(b) and an improved gain of 7.72 dBi is achieved.

4) STAGE 4

To improve the isolation between the 5G and 4G feeders, a LPF is added as shown in Fig. 4(d). The LPF is designed based on a stepped impedance method, where the LPF consists of alternating sections of very high and very low characteristic impedance lines [20]. The performance of the LPF is shown in Fig. 5. The simulated reflection coefficient, which describes how much of an electromagnetic signal is reflected from an antenna, and isolation curves for 5G/4G bands after adding the LPF are shown in Fig. 3(c) and Fig. 3(d). It is clear that isolation and impedance matching bandwidth is improved significantly after adding the LPF. It covers the 25-40 GHz band with a maximum gain of 8 dBi at 38 GHz. The maximum realized gain at stages 1 to 4 is 9.1, 5.9, 7.7, and 7.9 dBi, respectively.

III. RESULT AND DISCUSSION

In this part, the results are discussed for the 4-element MIMO antenna system. Optimization is used to ensure the best performance at low and high frequencies. A fabrication is realized to verify the proposed antenna structure. The photograph of the fabricated prototype is shown inside Fig. 7.

A. INTEGRATED 5G/4G MIMO ANTENNA SYSTEM

The geometry of the proposed MIMO antenna system is shown in Fig. 1. It consists of four antenna elements (Ant-1-Ant-4) and 8-feeders (F1, F3, F5 and F7 for 4G and F2, F4, F6 and F8 for 5G). Due to the placement of the MIMO antennas on the four sides of the substrate (orthogonal to each other), spatial diversity is achieved, leading to high isolation between MIMO antenna elements especially at the 4G band. Antenna placement or orientation technique is well known to increase the isolation between MIMO antenna elements [21], [22]. The size of the substrate is similar to the size of the latest smart phones. The length of both feeders (5G and 4G)

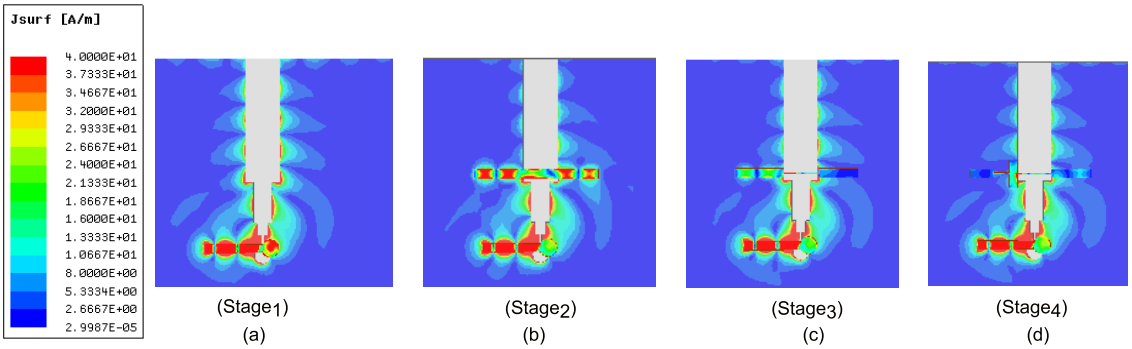

FIGURE 4. Current distributions at different stages ($Stage_1$-$Stage_4$) of the 4G feeder at 38 GHz.

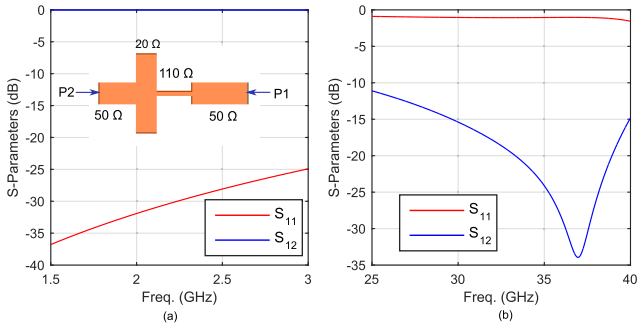

FIGURE 5. Performance of low pass filter at (a) 4G band, and (b) 5G band.

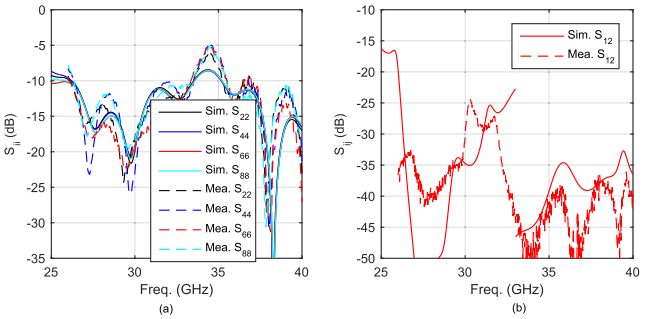

FIGURE 6. Simulated and measured S-parameters for 5G band. (a) S_{ii}, and (b) S_{ij}.

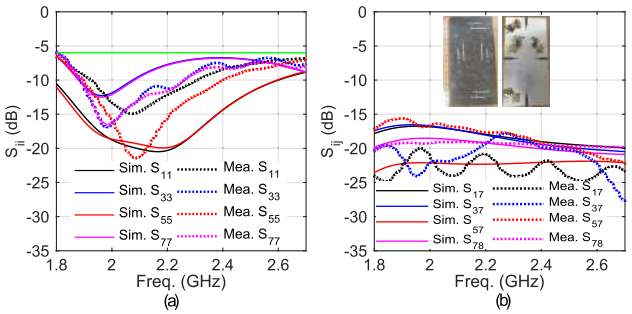

FIGURE 7. Simulated and measured S-parameters for 4G band. (a) S_{ii}, and (b) S_{ij}.

are extended to integrate 50Ω SMA and mm-Wave connectors and to have enough space for antenna testing.

While adding all antenna elements to sides of the substrate, performance remains unchanged at 5G bands. However, at the 4G bands, Ant-1 and Ant-2 have slightly different reflection coefficients as shown in Fig. 7(a) (S_{11} and S_{33}). This difference is caused by the size of the ground plane [23]. These antennas have different ground plane sizes, i.e. Ant-1 has a width W_{sub}, while Ant-2 has a width L_{sub} (as shown in Fig. 1). However, the proposed design still has good impedance matching below −6 dB, and this is acceptable for 4G applications [9].

1) PORT PARAMETERS

The simulated and measured reflection coefficient curves for the 5G band are shown in Fig. 6(a). The results show that the proposed 5G antennas cover the 25-40 GHz frequency band. Fig. 6(b) shows isolation curves between F1 and F2. A minimum of 25 dB measured isolation is observed across the whole covered band. Isolation between the 5G ports (F2, F3, F5 and F7) is observed to be more than 50 dB.

The simulated and measured reflection coefficient curves for the 4G band are shown in Fig. 7(a). The results show that the proposed design covers 1.8-2.6 GHz band with -6 dB impedance matching bandwidth. The slight differences between the simulated and measured S_{11} and S_{33} can be attributed to fabrication tolerances. Fig. 7(b) shows the isolation curves between various ports of 4G and 5G. A minimum of 16 dB measured isolation is observed between F5 and F7.

An important aspect of this design is that the polarization of Ant-1 and Ant-3 is perpendicular to Ant-2 and Ant-4. Since the electric field of the tapered slot antenna is perpendicular to the slot orientation, the polarization of Ant-1 and Ant-3 is along the y-direction, whereas the polarization of Ant-2 and Ant-4 is along the x-direction. This polarization diversity improves the isolation of the MIMO elements. In addition, this type of antenna diversity also improves the reliability of the mobile network and thus, enhances its data rate.

2) RADIATION PATTERNS

The simulated and measured radiation patterns are obtained when one antenna is excited and others are terminated with a match load of 50 Ω [14].

The normalized two-dimensional (2D) radiation patterns for 5G bands are shown in Fig. 8 and Fig. 9 for Ant-1 and

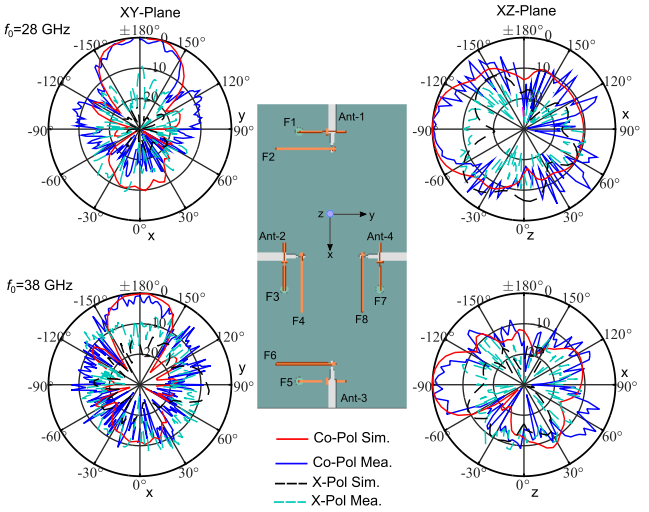

FIGURE 8. Normalized simulated and measured radiation patterns at different frequencies for 5G bands (Ant-1).

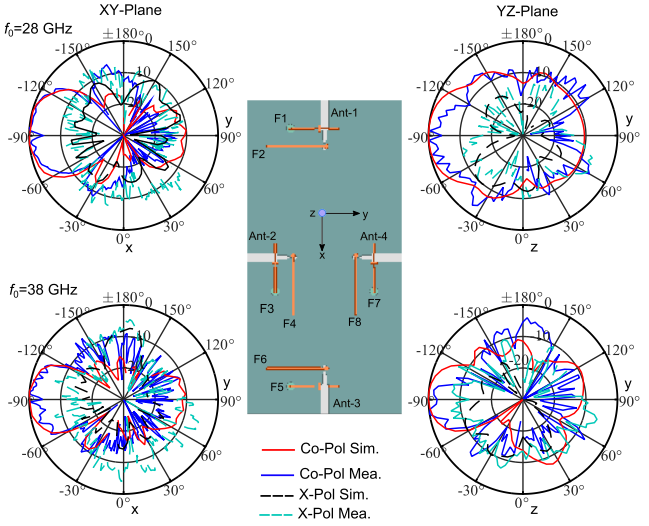

FIGURE 9. Normalized simulated and measured radiation patterns at different frequencies for 5G bands (Ant-2).

TABLE 1. Simulated and measured peak gain for 5G band.

Peak gain (dBi)	27.5 GHz	28 GHz	38 GHz	39 GHz
Simulated	5.8	6.2	7.6	7.2
Measured	5.5	5.1	7	7.2

Ant-2 at 28 and 38 GHz frequencies, respectively. Due to the symmetry in the design, only the radiation patterns for Ant-1 and Ant-2 are shown. Both antennas have strong radiation patterns in different directions in the xy-plane, i.e. Ant-1 has a maximum value at $\phi = 180°$, while Ant-2 at $\phi = -90°$. Such radiation patterns are desirable for MIMO applications and provide un-correlated communication channels.

The normalized 2D radiation patterns for the 4G band are shown in Fig. 10 for Ant-1 and Ant-2 at 2.0 GHz. Both

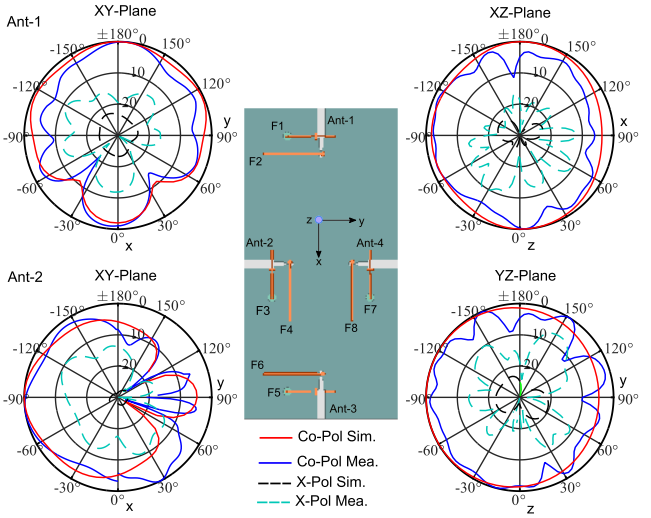

FIGURE 10. Normalized simulated and measured radiation patterns for 4G band.

TABLE 2. Simulated and measured peak gain for 4G band.

Peak gain (dBi)	1.8 GHz	2.0 GHz	2.3 GHz	2.6 GHz
Simulated	3.7	3.3	2.5	3.6
Measured	3.6	3.1	2.4	2.9

antennas have directional radiation patterns in the xy-plane, i.e. Ant-1 has directive beam towards $\phi = 180°$, while Ant-2 towards $\phi = -90°$. Whereas, in xz and yz planes, both of them show omni-directional radiation patterns.

The simulated and measured peak gain values are shown in Table 1 and Table 2 for 5G and 4G bands, respectively. The maximum measured value is observed to be 7.2 dBi at 39 GHz for the 5G band, whereas for the 4G band, the maximum measured gain is 3.6 dBi at 1.8 GHz. A slight difference between simulated and measured values is observed due to the measurement errors. The proposed design has a measured efficiency of 60-85% and 70-90% at the 5G and 4G bands, respectively, where the efficiency represents the ratio of the radiated power by a MIMO antenna element to the input power. Based on the aforementioned results, the proposed design offers a directive pattern for the 5G, which is needed to compensate the high path loss at mm-Wave band. It also uses one structure for 5G and 4G antenna, which ensures sufficient space for other components inside the handset.

B. EFFECTS OF LCD AND HAND/HEAD PHANTOM

Since the positions of MIMO antennas are located on the edges of the ground plane, the influence of adding a Liquid Crystal Display (LCD) is investigated through HFSS simulations. A large-size touch screen LCD with dimension 136×68 mm^2 are located underneath the ground plane. The LCD is assumed to be a perfect electric conductor (PEC) for the proposed design [24]. The simulated and measured reflection coefficient and efficiency of MIMO antenna are

TABLE 3. Comparison between proposed and reported 5G/4G MIMO antenna systems.

Ref.	Integrated 5G/4G in Same Structure	Support mm-Wave band	Size of Each Antenna Element (mm^2)	BW (GHz)	Realized Gain (dBi) at mm-Wave	Isolation (dB)	Hand/Head Phantom Integration in the Simulation
[9]	No	No	N/A	1.9-3.5 16.5-17.8	N/A	≥ 5	No
[10]	Yes	No	15×2.5 (5G/4G)	3.4-3.8 5.15-5.92	N/A	≥ 11	Yes
[13]	No	No	16×3 (5G) 30×9 (4G)	0.824-0.96 1.7-2.69 3.4-3.6	N/A	≥ 10	No
[14]	No	No	15×12 (5G) 7×3 (4G)	3.4-3.8 5.15-5.92	N/A	≥ 12	Yes
[15]	No	No	35×18.5 (5G) 24.6×6 (4G)	2-2.2 12.25-12.75	N/A	≥ 13.5	No
[16]	No	Yes	23×22.2 (5G) 25.4×7.9 (4G)	1.85-2.53 26-28.4	8	≥ 10	No
This Work	**Yes**	**Yes**	25×12 **(5G/4G)**	**1.8-2.6** **25-40**	**7.2**	≥ 17	Yes

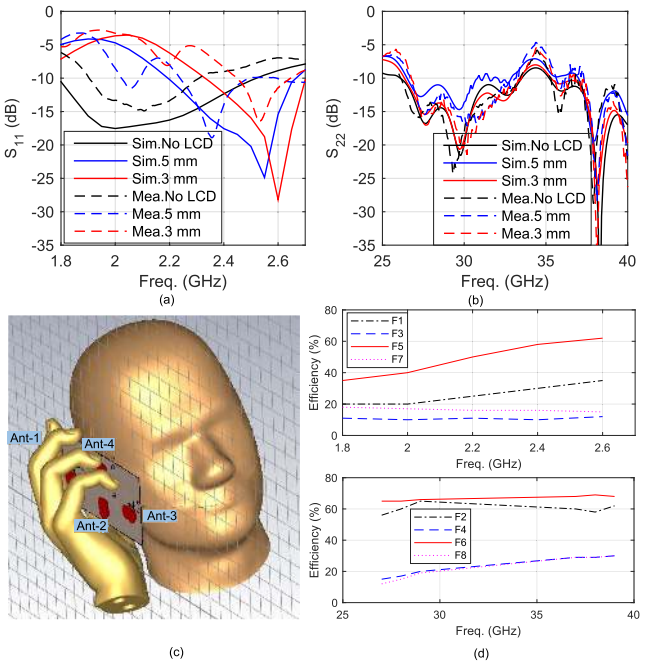

FIGURE 11. Effect of LCD and hand/head phantoms on proposed design (a) 4G band, (b) 5G band at different spacings between the LCD and the ground plane, (c) hand/head model, and (d) radiation efficiencies at 4G (top) and 5G (bottom) bands.

investigated for 3 mm, and 5 mm gap between the LCD and ground plane. For the sake of brevity, only the performance of Ant-1 is shown in Fig. 11(a) and Fig. 11(b), and the antenna performance without LCD is included for comparison purpose. As seen in Fig. 11, the performance after placing the LCD is still preserved at the 4G and 5G bands. However, it can be noticed that the 4G bandwidth is shifted towards the higher frequency by 0.2 GHz, compared to the ones without LCD (Fig. 11(a)) Fig. 11(b)). This shift can be fixed by reducing the value of L_{edge} from 13.5 mm to 10.5 mm. In addition, it is also noticed that the measured efficiency is degraded by 2-10% at the 4G band and by only 2% at the 5G band.

To analyze the influence of head/hand phantoms, CST Microwave Studio and the simulation model is used as shown in Fig. 11(c) while efficiency curves are shown in Fig. 11(d). It can be seen that Ant-2 and Ant-4, which are closely related to the head/hand phantom, are most affected, while the influence of the head/hand on Ant-1 and Ant-3, which are relatively far from the phantoms, is less significant. Ant-1 and Ant-3 still work well with maximum radiation efficiency of 65% and 60% at 28 and 2.6 GHz, respectively. Nevertheless, Ant-2 is the most affected in terms of antenna efficiency (a similar behaviour was observed in [14]). Compared with Ant-1, Ant-2 has a reduction on the efficiency of about -4 dB and -7 dB in the 5G and 4G bands respectively. This is due to the significant amount of field absorption into the hand/head phantom and the locations of four antennas with respect to the phantoms. Based on the simulation setup in Fig. 11(c), the SAR value is 0.83 W/kg when the input power of each MIMO element is set to be 24 dBm, which is the maximum user equipment output power used for evaluating the SAR value of the 4G technology. While, at mm-Wave 5G and based on the International Commission on Non-Ionizing Radiation Protection (ICNIRP), the power density is used to measure the absorbed power instead of the SAR. It is found that the power density is 46.5 W/m^2 over 1 cm^2 an averaging area at 5G band. Both the SAR and power density values satisfy the current ICNIRP limit of 1.6 W/Kg and 200 W/m^2, respectively [25], [26]. In terms of realized gain and directivity, the realized gain varies by about 1 dBi, while the directivity varies by around 2 dB. However, utilizing MIMO allows for a spatial diversity, which means that even if the body blocks the signal or the connection of one or more of the MIMO antenna elements, the other elements can still work and it thus enables MIMO operation.

C. MIMO PARAMETERS CALCULATIONS

MIMO parameters such as Envelope Correlation Coefficient (ECC), Channel Capacity (CC), and Mean Effective Gain (MEG) are also calculated to show MIMO performance. The Envelope Correlation Coefficient (ECC) parameter is used to serve diversity performance [14]. It is calculated based on the three-dimensional (3D) farfield radiation patterns between

antenna pairs at low and high frequencies using the following equation [15].

$$\rho_e = \frac{|\int\int_0^{4\pi}[\vec{F}_1(\theta,\phi)\times\vec{F}_2(\theta,\phi)]d\Omega|^2}{\int\int_0^{4\pi}|\vec{F}_1(\theta,\phi)|^2 d\Omega \int\int_0^{4\pi}|\vec{F}_2(\theta,\phi)|^2 d\Omega} \quad (1)$$

where, $\vec{F}_1(\theta,\phi)$ and $\vec{F}_2(\theta,\phi)$ are the 3D radiated fields of Ant-1 and Ant-2, respectively, while Ω is the solid angle. The maximum value of ECC was found to be lower than 0.001 at both bands (5G/4G) which is much lower than the maximum ECC acceptable threshold of 0.5. In addition, the CC is calculated using the following equation [27].

$$CC = log_2\left(det\left[I + \frac{SNR}{N}HH^*\right]\right) \quad (2)$$

where, I is the identity matrix of $N \times N$ dimensions, SNR is the signal to noise ratio and H is the channel matrix that contains radiation characteristics of the MIMO antenna elements and channel environment. It is assumed that the power is equally divided between the transmitting elements of the MIMO system. In this study, H is calculated using the Kronecker model which is demonstrated in [27]. It is observed that the maximum CC of 10.5 bps/Hz is achieved with 4×4 MIMO configuration at 20 dB SNR, while the ideal CC for 4×4 MIMO is 18.8 bps/Hz at both 4G/5G bands. The MEG of the proposed design is also calculated based on 3D radiation patterns. It is assumed that the 3D power distribution function is defined as a Gaussian for elevation plane while uniform for azimuth plane, and the cross polarization ratio (XPR) is equal to 2 dB (corresponds to an ordinary fading environment [28]), the MEG remains about -4.5 dB with the variation of less than 1 dB for all MIMO antenna elements at both frequency bands meaning that the proposed design has acceptable MIMO performance.

D. PERFORMANCE COMPARISON WITH CURRENT 4G AND 5G ANTENNAS

To make the merits of the proposed design explicit, a comparison table is carried out with recent published 5G/4G MIMO antenna systems for mobile applications as shown in Table 3. The proposed design is compared with other MIMO antenna systems in terms of the integration of 5G and 4G in the same structure, supporting mm-Wave band, MIMO element size, bandwidth, realized gain, isolation, and user's hand or head effects. However, building mm-Wave 5G and 4G antenna in the same structure is a new topic, and the reported designs on this topic, in the literature are rare. Therefore, table 3 makes it clear that the proposed design has a unique feature of integrating mm-Wave 5G and 4G antennas in the same structure, while other designs do not. However, the integration of the 5G and 4G structure is achieved in [10] with small size but it only covers sub-7 GHz band. Although [16] covers similar bands (mm-Wave and 2 GHz band), it deploys separate structures having larger sizes.It uses 23×22 mm^2 for 5G and 23.5×9 mm^2 for 4G compared with the proposed design that has only 25×12 mm^2 size for both 5G and 4G. All other antenna designs [9], [13]–[15] cover different bands (excluding mm-Wave) bands with variations in the realized gain and isolation of MIMO elements. Overall, this design provides a novel antenna integration strategy for future mm-Wave 5G with existing 4G technologies in a single structure.

IV. CONCLUSION

A 4-element MIMO antenna system for 5G/4G mobile technology has been demonstrated. By utilizing a ground tapered slot and two microstrip feeders, the design can work as a tapered slot antenna for 5G, covering 27.5-40 GHz or as an open-ended slot antenna for 4G covering 1.8-2.6 GHz. Its planar footprint and wide bandwidth features make it a good candidate for 5G/4G handheld devices. The design has an isolation of more than 25 dB at mm-Wave and 16 dB at the 2 GHz band. The design has a directive radiation patterns with a gain of 7 dBi at mm-Wave and isotropic radiation patterns with a gain of 3 dBi at the 2 GHz band. The calculated ECC and isolation values meet the requirements of MIMO systems. As a proof of concept is demonstrated in the presented work, adding a beam steering capability to the design will be explored in the future.

REFERENCES

[1] H. T. Chattha, "4-port 2-element mimo antenna for 5G portable applications," *IEEE Access*, vol. 7, pp. 96516–96520, 2019.
[2] J. Guo, L. Cui, C. Li, and B. Sun, "Side-edge frame printed eight-port dual-band antenna array for 5G smartphone applications," *IEEE Trans. Antennas Propag.*, vol. 66, no. 12, pp. 7412–7417, Dec. 2018.
[3] N. O. Parchin, Y. I. A. Al-Yasir, A. H. Ali, I. Elfergani, J. M. Noras, J. Rodriguez, and R. A. Abd-Alhameed, "Eight-element dual-polarized MIMO slot antenna system for 5G smartphone applications," *IEEE Access*, vol. 7, pp. 15612–15622, 2019.
[4] M. Ikram, N. Nguyen-Trong, and A. Abbosh, "Multiband MIMO microwave and millimeter antenna system employing dual-function tapered slot structure," *IEEE Trans. Antennas Propag.*, vol. 67, no. 8, pp. 5705–5710, Aug. 2019.
[5] E. Al Abbas, A. M. Abbosh, and K. Bialkowski, "Tunable in-phase power divider for 5G cellular networks," *IEEE Microw. Wireless Compon. Lett.*, vol. 27, no. 6, pp. 551–553, Jun. 2017.
[6] T. S. Rappaport, S. Sun, R. Mayzus, H. Zhao, Y. Azar, K. Wang, G. N. Wong, J. K. Schulz, M. Samimi, and F. Gutierrez, "Millimeter wave mobile communications for 5G cellular: It will work!" *IEEE Access*, vol. 1, pp. 335–349, 2013.
[7] B. Xu, K. Zhao, Z. Ying, D. Sjöberg, W. He, and S. He, "Analysis of impacts of expected RF EMF exposure restrictions on peak EIRP of 5G user equipment at 28 GHz and 39 GHz bands," *IEEE Access*, vol. 7, pp. 20996–21005, 2019.
[8] W. Hong, "Solving the 5G mobile antenna puzzle: Assessing future directions for the 5G mobile antenna paradigm shift," *IEEE Microw. Mag.*, vol. 18, no. 7, pp. 86–102, Nov. 2017.
[9] M. S. Sharawi, M. Ikram, and A. Shamim, "A two concentric slot loop based connected array MIMO antenna system for 4G/5G terminals," *IEEE Trans. Antennas Propag.*, vol. 65, no. 12, pp. 6679–6686, Dec. 2017.
[10] Y. Li, C.-Y.-D. Sim, Y. Luo, and G. Yang, "Multiband 10-antenna array for sub-6 GHz MIMO applications in 5-G smartphones," *IEEE Access*, vol. 6, pp. 28041–28053, 2018.
[11] M.-Y. Li, Z.-Q. Xu, Y.-L. Ban, C.-Y.-D. Sim, and Z.-F. Yu, "Eight-port orthogonally dual-polarised MIMO antennas using loop structures for 5G smartphone," *IET Microw., Antennas Propag.*, vol. 11, no. 12, pp. 1810–1816, 2017.
[12] S. Chen, P. Wu, C. G. Hsu, and J. Sze, "Integrated MIMO slot antenna on laptop computer for eight-band LTE/WWAN operation," *IEEE Trans. Antennas Propag.*, vol. 66, no. 1, pp. 105–114, Jan. 2018.

[13] Y.-L. Ban, C. Li, C.-Y.-D. Sim, G. Wu, and K.-L. Wong, "4G/5G multiple antennas for future multi-mode smartphone applications," *IEEE Access*, vol. 4, pp. 2981–2988, 2016.
[14] Y. Li, C.-Y.-D. Sim, Y. Luo, and G. Yang, "12-Port 5G massive MIMO antenna array in Sub-6 GHz mobile handset for LTE bands 42/43/46 applications," *IEEE Access*, vol. 6, pp. 344–354, 2017.
[15] M. Ikram, R. Hussain, and M. S. Sharawi, "4G/5G antenna system with dual function planar connected array," *IET Microw., Antennas Propag.*, vol. 11, no. 12, pp. 1760–1764, 2017.
[16] R. Hussain, A. T. Alreshaid, S. K. Podilchak, and M. S. Sharawi, "Compact 4G MIMO antenna integrated with a 5G array for current and future mobile handsets," *IET Microw., Antennas Propag.*, vol. 11, no. 2, pp. 271–279, 2017.
[17] K. Ebnabbasi, D. Busuioc, R. Birken, and M. Wang, "Taper design of Vivaldi and co-planar tapered slot antenna (TSA) by Chebyshev transformer," *IEEE Trans. Antennas Propag.*, vol. 60, no. 5, pp. 2252–2259, May 2012.
[18] U. T. Ahmed and A. M. Abbosh, "In-phase power divider with three octaves band using microstrip to slotline transitions and loosely coupled microstrip lines," in *Proc. Asia–Pacific Microw. Conf. (APMC)*, vol. 2, Dec. 2015, pp. 1–3.
[19] Y. Xu, J. Wang, L. Ge, X. Wang, and W. Wu, "Design of a notched-band Vivaldi antenna with high selectivity," *IEEE Antennas Wireless Propag. Lett.*, vol. 17, pp. 62–65, 2018.
[20] J. Ni and J. Hong, "Compact continuously tunable microstrip low-pass filter," *IEEE Trans. Microw. Theory Techn.*, vol. 61, no. 5, pp. 1793–1800, May 2013.
[21] H. Li, B. K. Lau, Z. Ying, and S. He, "Decoupling of multiple antennas in terminals with chassis excitation using polarization diversity, angle diversity and current control," *IEEE Trans. Antennas Propag.*, vol. 60, no. 12, pp. 5947–5957, Dec. 2012.
[22] M. Pelosi, M. B. Knudsen, and G. F. Pedersen, "Multiple antenna systems with inherently decoupled radiators," *IEEE Trans. Antennas Propag.*, vol. 60, no. 2, pp. 503–515, Feb. 2012.
[23] K.-L. Wong and C.-Y. Tsai, "Low-profile dual-wideband inverted-T open slot antenna for the LTE/WWAN tablet computer with a metallic frame," *IEEE Trans. Antennas Propag.*, vol. 63, no. 7, pp. 2879–2886, Jul. 2015.
[24] Q. Guo, R. Mittra, F. Lei, Z. Li, J. Ju, and J. Byun, "Interaction between internal antenna and external antenna of mobile phone and hand effect," *IEEE Trans. Antennas Propag.*, vol. 61, no. 2, pp. 862–870, Feb. 2013.
[25] K. Zhao, Z. Ying, and S. He, "EMF exposure study concerning mmWave phased array in mobile devices for 5G communication," *IEEE Antennas Wireless Propag. Lett.*, vol. 15, pp. 1132–1135, 2016.
[26] W. He, B. Xu, M. Gustafsson, Z. Ying, and S. He, "RF compliance study of temperature elevation in human head model around 28 GHz for 5G user equipment application: Simulation analysis," *IEEE Access*, vol. 6, pp. 830–838, 2018.
[27] Z. Li, Z. Du, M. Takahashi, K. Saito, and K. Ito, "Reducing mutual coupling of MIMO antennas with parasitic elements for mobile terminals," *IEEE Trans. Antennas Propag.*, vol. 60, no. 2, pp. 473–481, Feb. 2012.
[28] M.-Y. Li, Y.-L. Ban, Z.-Q. Xu, J. Guo, and Z.-F. Yu, "Tri-polarized 12-antenna MIMO array for future 5G smartphone applications," *IEEE Access*, vol. 6, pp. 6160–6170, 2017.

EMAD AL ABBAS (S'15) received the M.Sc. degree in electrical engineering from the University of Baghdad, Iraq. He is currently pursuing the Ph.D. degree in electrical engineering with The University of Queensland (UQ), Brisbane, QLD, Australia. Before his Ph.D., he was an RF Senior Unit Head of the Ooredoo Telecommunication Company, Iraq. He is also a member of the Electromagnetic Innovations ($\mathcal{E}$MAGin) Group, UQ. His research interests include antenna design, reconfigurable antennas, and MIMO antennas for mobile smartphone, as well as wireless communication systems.

MUHAMMAD IKRAM (S'19) received the B.Sc. and M.Sc. degrees in electrical engineering from the University of the Punjab, Pakistan, and the King Fahd University of Petroleum and Minerals (KFUPM), Saudi Arabia, in 2014 and 2017, respectively. He is currently pursuing the Ph.D. degree in electrical engineering with the School of Information Technology and Electrical Engineering (ITEE), The University of Queensland (UQ), Brisbane, QLD, Australia. He is also a member of the Electromagnetic Innovations ($\mathcal{E}$MAGin) Group, UQ. His current research interests include integrated multiple-input multiple-output (MIMO) antenna designs for 4G/5G mobile handsets and future wireless devices, antenna arrays, frequency reconfigurable antennas, and mobile communications.

AHMED TOAHA MOBASHSHER was born in Chittagong, Bangladesh. He received the B.Sc. degree in electrical and electronic engineering from the Chittagong University of Engineering and Technology, Chittagong, Bangladesh, in 2008, the M.Sc. (by research) degree from the Department of Electrical, Electronic and Systems Engineering, Universiti Kebangsaan Malaysia, Malaysia, in 2011, and the Ph.D. degree from the School of IT and Electrical Engineering (ITEE), The University of Queensland (UQ), Brisbane, Australia, in 2016, where he is currently working as a UQ Development Fellow. His research interests include antenna development for microwave imaging, head imaging, ultrawideband (UWB) imaging, human tissue equivalent phantoms, 3-D phantoms, RFID reader, design of compact, multiband and wideband antennas, notched ultrawide band antennas, metamaterial antennas, and antenna miniaturization.

AMIN ABBOSH (SM'08) leads the Electromagnetic Innovations ($\mathcal{E}$MAGin) Group, and is also the Head of the School of Information Technology and Electrical Engineering, The University of Queensland, Australia. He has authored more than 400 articles on electromagnetic imaging systems for medical applications, wideband passive microwave devices, and planar antennas. As a recognition of his international research standing, he received the higher doctorate (Doctor of Engineering) from the University of Queensland, in 2013. For his leading role in mentioning Ph.D. students, he was awarded UQ's Excellence in Supervision (2016). He is an Associate Editor for the IEEE TRANSACTIONS ON ANTENNAS AND PROPAGATION, and the Senior Associate Editor for the IEEE ANTENNAS AND WIRELESS PROPAGATION LETTERS.